Fast Mask Image Projection-Based Micro-Stereolithography Process for Complex Geometry

Yayue Pan[1]
Mem. ASME
Department of Mechanical and Industrial Engineering,
University of Illinois at Chicago,
842 W. Taylor Street,
ERF 2039,
Chicago, IL 60607
e-mail: yayuepan@uic.edu

Yong Chen
Mem. ASME
Epstein Department of Industrial and Systems Engineering,
University of Southern California,
3715 McClintock Avenue,
GER 201,
Los Angeles, CA 90089
e-mail: yongchen@usc.edu

Zuyao Yu
School of Ship and Ocean Engineering,
Huazhong University of Science and Technology,
1037 Luoyu Road,
East Building 2-118,
Wuhan 430074, Hubei
e-mail: yuzuyao@163.com

In micro-stereolithograhy (μSL), high-speed fabrication is a critical challenge due to the long delay time for refreshing resin and retaining printed microfeatures. Thus, the mask-image-projection-based micro-stereolithograhy (MIP-μSL) using the constrained surface technique is investigated in this paper for quickly recoating liquid resin. It was reported in the literature that severe damages frequently happen in the part separation process in the constrained-surface-based MIP-μSL system. To conquer this problem, a single-layer movement separation approach was adopted, and the minimum delay time for refreshing resin was experimentally characterized. The experimental results verify that, compared with the existing MIP-μSL processes, the MIP-μSL process with single-layer movement separation method developed in this paper can build microstructures with complex geometry, with a faster build speed. [DOI: 10.1115/1.4035388]

1 Introduction

The MIP-μSL technology is an additive manufacturing (AM) approach for fabricating microstructures with three-dimensional (3D) complex geometry, especially with high aspect ratios [1–5]. Compared with other micro-manufacturing technologies such as lithography gavolnoforming abforming (LIGA) and micromachining [6,7], MIP-μSL technology has the merits of simpler processing, faster fabrication speed, lower machine cost, and better capability of fabricating complex geometry. Various applications of MIP-μSL have been investigated, including the fabrication of microfluidic devices, scaffolds of biocompatible polymers for tissue reconstruction, microrobotics, etc. [8–11]. To fabricate a micropart using MIP-μSL, first, a 3D computer-aided design (CAD) model is sliced to generate a set of two-dimensional (2D) layers. Each sliced layer is saved as a digital mask image, which is then projected usually by a digital micromirror device (DMD) to cure a thin layer of liquid resin [10–15]. The smallest feature reported by the MIP-μSL process is 0.6 μm [11]. Most MIP-μSL systems use a top–down projection approach. Related MIP-μSL systems based on the top–down projection approach are illustrated in Fig. 1(*a*). A good property of the top–down projection approach is that top surface of the cured layers is free, making it always feasible to recoat a new layer of liquid resin on top of the cured layer. However, when the needed new layer of liquid resin becomes thin, the recoating process becomes more challenging and sometimes even impossible, because of the liquid viscosity and surface tension. A resin recoating process based on a sweeper is usually required to flatten the top surface. For low-viscosity resins, a deep-dip recoating approach with a long waiting time can also be used to replace the surface sweeping process.

In comparison, a schematic diagram of the MIP-μSL systems based on bottom–up projection is shown in Fig. 1(*b*). Although the bottom–up projection-based MIP-μSL systems have now been widely used to fabricate macroscale structures, a relatively less literature [10] was reported to fabricate microstructures using such a constrained-surface-based approach. As a cured layer is constrained by the tank surface, it is found that the separation of the cured part is a critical issue, especially when it has microfeatures. The fabricated microstructure can be broken easily during the layer separation process. Hence, the adoption of such bottom–up projection approach in microstructure fabrication is greatly limited due to the layer separation.

In this paper, we discuss how to achieve fast build speed in the MIP-μSL process based on the bottom–up projection method. We tried to minimize the resin refreshing time by utilizing the bottom–up projection configuration and a single-layer movement separation approach. A testbed was developed and experiments were performed for various geometries to validate the developed MIP-μSL approaches.

2 A Fast MIP-μSL Process Design

2.1 Fast MIP-μSL Process Based on Bottom–Up Projection. It is found that a large separation force may occur and bubbles will be generated during the separation process, especially when a small layer thickness and a fast separating speed are used. Therefore, a 2-mm thick flexible layer of polydimethylsiloxane (PDMS, Sylgard 184 from Dow Corning, Midland, MI) is coated on the bottom surface of the liquid vat to assist the separation [16,17]. After projecting a mask image through the bottom surface of the liquid vat for a certain time and curing a layer of resin, the platform is moved up with a proper velocity along the *Z*

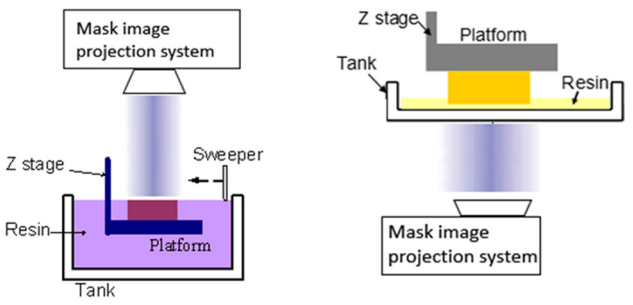

Fig. 1 Schematic of MIP-μSL systems based on the top–down projection method (*a*) and the bottom–up projection method (*b*)

[1]Corresponding author.

Contributed by the Manufacturing Engineering Division of ASME for publication in the Journal of Micro- and Nano-Manufacturing. Manuscript received April 19, 2016; final manuscript received November 30, 2016; published online January 6, 2017. Assoc. Editor: Cheryl Xu.

direction by a certain distance. Enough waiting time is necessary to ensure the complete filling of liquid resin in the gap with no bubbles existing. Since for a given setup with a preselected liquid resin, process parameters such as layer thickness, light intensity, and resin curing time can be determined for the MIP-SL process; a significant portion of the MIP-μSL fabrication time that can be adjusted through process control is the resin recoating time. Therefore, to achieve a fast building process, the process parameters that determine resin recoating are critical, which are investigated in the paper including the moving-up distance and the delay time for complete filling of liquid resin. They are further minimized through experimental study for a fast MIP-μSL process.

2.2 Experimental Study of Parameters Settings. In bottom–up projection-based MIP-μSL process, fresh liquid may not be able to fill the gap completely in time, and bubbles may be generated in the liquid-filling process if the separation speed is too high. A long waiting time and a big moving distance would guarantee a complete filling of liquid resin in the gap; however, the building time will be longer. Hence, it is desired to identify the shortest waiting time and smallest moving distance in order to achieve a fast fabrication speed. To identify the minimum waiting time needed to guarantee a complete filling of liquid resin, a prototype has been developed, as discussed in Sec. 3, and the experiments have been performed based on it.

Cubes with various sizes are built by using different waiting times and moving distances for a commercial resin (SI500 from EnvisionTec) with a viscosity of 200 cP. For example, Fig. 2 shows a cube model of $6.96 \times 6.96 \times 2$ mm^3. If the built parts have holes or deep shadows under a microscope, the waiting time is considered insufficient. Accordingly, a longer waiting time will be used to rebuild the parts. A critical waiting time for void-free curing is identified for different gap sizes.

Figure 3 plots the relation between the critical waiting time, the cube size, and the Z movement distance. In all the tests, the same Z movement speed (0.05 mm/s) was used to lift the platform up. It can be observed that:

(1) The minimum waiting time increases with the dimensional size for the same gap height, and bigger gap height results in a smaller minimum waiting time.
(2) When the cross section size of the cured layer is smaller than 6 mm, and the gap size is bigger than 10 μm, no waiting time is needed to get the gap completely filled by the tested liquid resin. However, when the solid cross section size of the cured layer is bigger than 6 mm, a minimum waiting time t_w is required in order to achieve nonvoid and bubble-free liquid resin filling. For the given setup, t_w can be determined by using the following fitted experimental model:

$$t_w = \begin{cases} 0 & x \le 6.01\,\text{mm} \\ 2.99h^2 - 14.07h + 16.46 & 6.01\,\text{mm} < x \le 6.45\,\text{mm} \\ 2.64h^2 - 14.56h + 20.96 & 6.45\,\text{mm} < x \le 6.99\,\text{mm} \end{cases} \quad (1)$$

where h is the gap height ($\times 10^{-5}$ m), and x is the solid cross section size of the layer.

2.3 Build Time of a Layer With the Single-Layer Movement Approach. According to the calibration tests for the preselected liquid resin, a single-layer separation and resin recoating process is developed by setting one-layer-thickness gap height and the minimum waiting time based on Eq. (1). Figure 4 presents

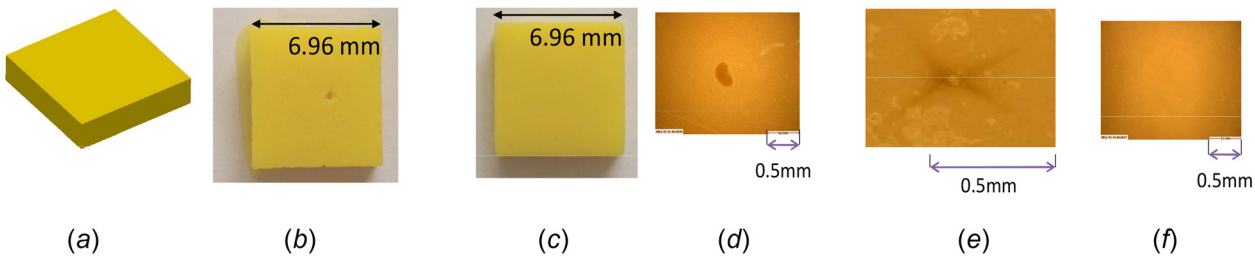

Fig. 2 Test results for identifying the minimum gap size and waiting time: (*a*) CAD model; (*b*) built part with insufficient waiting time; (*c*) void-free parts; (*d*) surface with a hole; (*e*) shadows due to incomplete filling; and (*f*) void-free surface

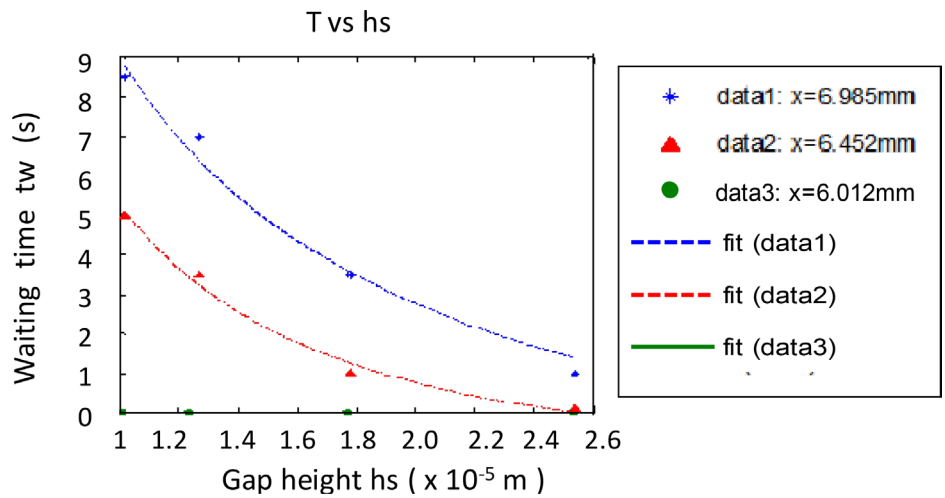

Fig. 3 The flow-filling time with different *Z* movement distance

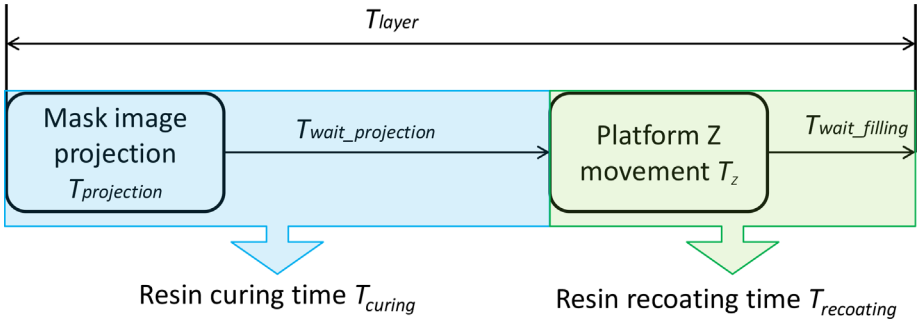

Fig. 4 Build time of a layer in a constrained-surface MIP-μSL process with the proposed single-layer movement approach

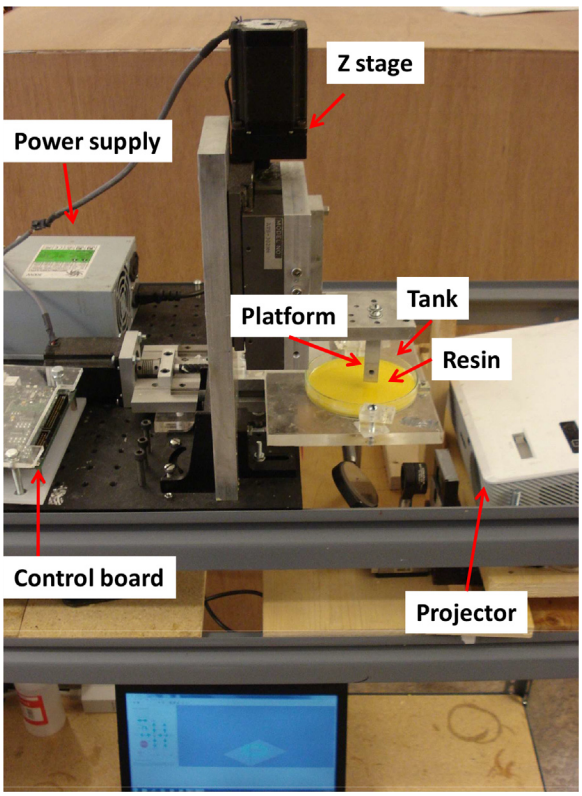

Fig. 5 Hardware setup of the developed MIP-μSL testbed

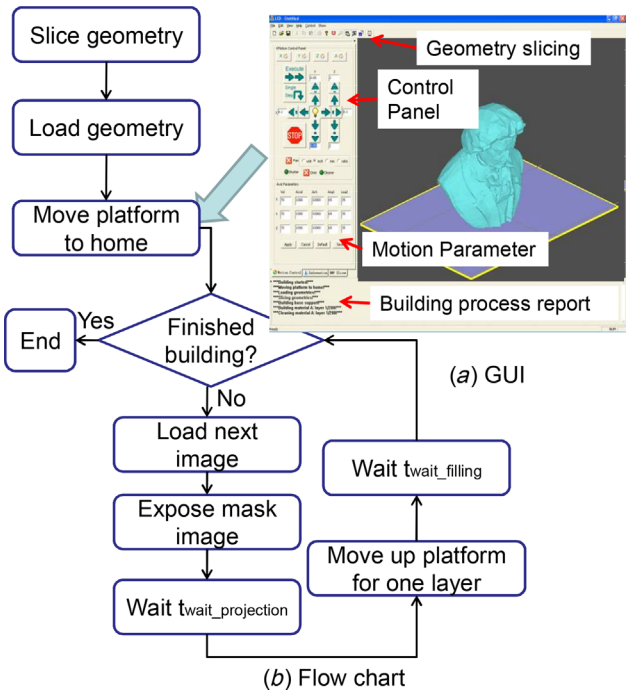

Fig. 6 Software setup of the developed fast micro-stereolithography and the related process flowchart

the build time of a layer using the proposed single-layer movement approach. It is the sum of all the following items: $T_{layer} = T_{curing} + T_{recoating} = (T_{projection} + T_{wait\_projection}) + (T_z + T_{wait\_filling})$. T_{curing} represents the time needed for curing resin completely, which is comprised of two portions, $T_{projection}$ and $T_{wait\_projection}$. T_{curing} is dependent on the light source, such as light intensity and wavelength, and the photo-sensitivities of the resin. The rest of the build time is used for separating the cured layer from the constrained surface and recoating a new layer of liquid resin for the next-layer curing. So we call it $T_{recoating}$, which is comprised of T_z and $T_{wait\_filling}$. As discussed before, the bottleneck for achieving a fast building speed is the resin recoating process [8,9,11,17,18]. With the goal of developing a method for achieving a fast build speed for a given MIP-μSL setup and used photocurable material, we focus on minimizing the resin recoating time, i.e., $T_{recoating}$. In this study, the following methods are used:

(1) We utilized a bottom–up projection configuration, which is widely adopted in macroscale stereolithography systems but not in micro-stereolithography systems.
(2) The platform is moved up by only a layer thickness to separate the newly cured layer and to allow resin fill in the gap, instead of using the conventional method of moving up a certain distance and then moving down to form a layer gap.
(3) An additional waiting time after the platform movement is added to complete the resin recoating process.

According to the experimental calibration in Sec. 2.2, the needed waiting time is 0 s, for printing a feature with solid cross section size x in the range of (0 mm, 6 mm), when a liquid resin with a viscosity, that is, not larger than 200 cP, a layer thickness of 20 μm, a velocity of 0.05 mm/s, and an acceleration of 0.005 mm/s^2 are used. For the fabrication of layers with solid cross section whose sizes are bigger than 6 mm, the optimum setting for $T_{wait\_filling}$ is determined by the experimental model of flow-filling time (refer to Eq. (1) in Sec. 2.2). Compared with the traditional MIP-μSL processes that usually require more than 15 s to recoat a new layer of liquid resin, this is a great reduction of build time, enabling a much faster building speed for microstructure fabrication.

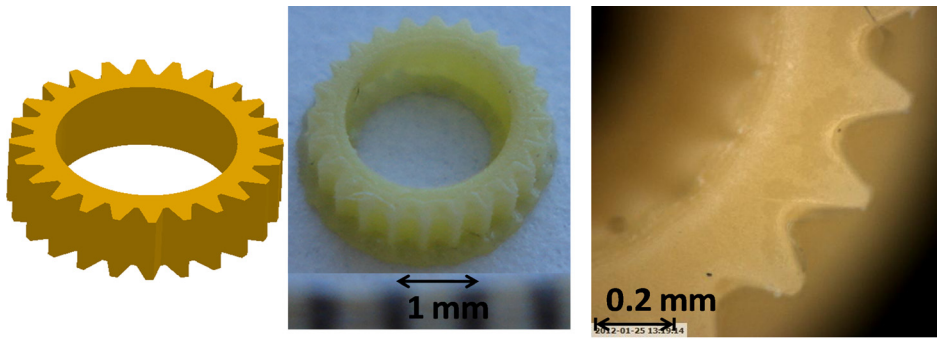

Fig. 7 A microgear: (*a*) CAD model; (*b*) built part; and (*c*) microscopic image

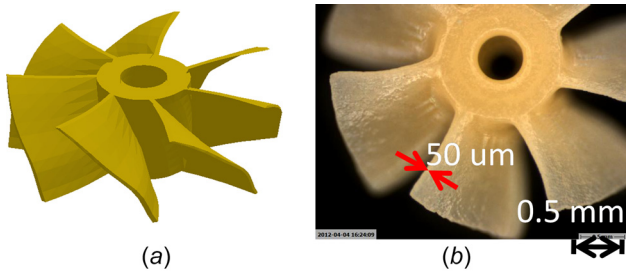

Fig. 8 A turbofan: (*a*) CAD model and (*b*) microscopic image of the built part

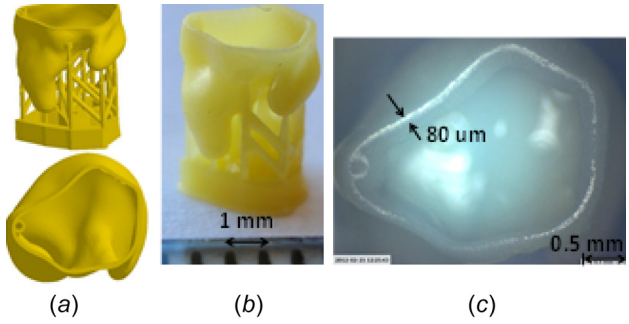

Fig. 9 A hearing-aid: (*a*) CAD model with added supports; (*b*) built physical object; and (*c*) microscopic image of the built part (top view)

3 Experimental Setup

As shown in Fig. 5, in order to verify the proposed micro-manufacturing approach, a hardware setup and a software have been built. A DMD-based projection device was developed by modifying a commercial projector from Acer. In particular, optical system settings, such as the projection image focus, light contrast, and light intensity, have been adjusted or modified to project a well-focused image on the liquid resin curing plane. A blue filter and a black mask are used to filter the light. A clear glass Petri dish coated with PDMS on the bottom is used as the resin tank. The envelope size is 9.32 mm $(X) \times 6.99$ mm $(Y) \times 50$ mm (Z). The projection image resolution of the prototype system is 9 μm. Note that by selecting different optics, e.g., light sources and lenses, larger or smaller build envelope size with different levels of resolution can be achieved in the MIP-μSL process. In addition, a process control software has been developed using Visual C++. It integrates the slicing, image loading, projection, and motion controlling, as shown in Fig. 6.

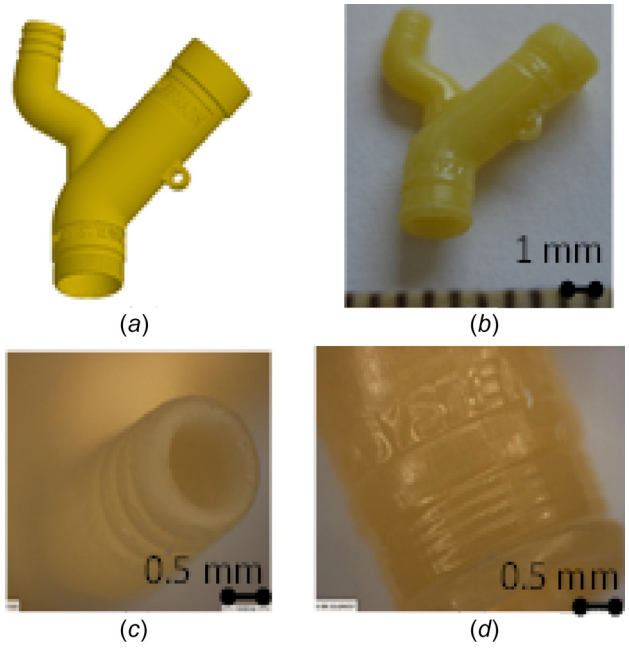

Fig. 10 A threaded pipe: (*a*) CAD model of the pipe and (*b*)–(*e*) built physical object

4 Experimental Results and Discussion

4.1 Test Cases. To calibrate the micro-manufacturing capability of the developed process, cylinders with varied diameters, and channels with varied sizes have been printed and characterized by measuring the fabricated microstructures using a precision measurement equipment from Micro-Vu (Windsor, CA) and comparing with the CAD model. It was found that the smallest pillar and the smallest gap that the system can build are 50 μm and 110 μm, respectively. The tolerance of the solid cylinders is around $\pm$ 4 μm, and the tolerance of the channel is around $\pm$ 10 μm. A contour elite 3D optical microscope from Bruker (Billerica, MA) was used to measure the surface roughness. The top surface of the printed cube in Fig. 2(*d*) has an average roughness (R_a) value of 0.1 μm. Other postprocess techniques such as chemical etching, post-curing, and meniscus approach can improve the precision and surface finish of fabricated objects.

To verify the capability of the system on building complex microstructures or mesoscale parts with microfeatures based on the fast printing method, various tests have been carried out for different geometries. CAD models, built parts, and the related microscopic images are shown in Figs. 7–10. In all the tests, $T_{\text{wait\_filling}}$ is determined by Eq. (1) in Sec. 2.2. If the calculated

Table 1 Performance of our newly developed MIP-μSL system

Model	Gear	Fan	Hearing-aid	Pipe
Figure #	Fig. 7	Fig. 8	Fig. 9	Fig. 10
Size x (mm)	2.96	5.867	3.05	8
Structure type	Solid	Curvature	Shell	Shell
Thickness (μm)	20	12	20	20
$T_{projection}$ (s)[a]	0.55	0.4	0.55	0.55
$T_{wait\_projection}$ (sec)	0.5	0.3	0.5	0.5
T_z (s)	3.06	2	3.06	3.06
$T_{wait\_filling}$ (s)	0.1	0.1	0.1	0.1
Height z (mm)	1	4.539	6.2	13.068
Layer #	50	378	310	653
T_{layer} (s) in our system	4.21	2.8	4.21	4.21
T_{layer} (s) in a commercial system	18.05	17	18.05	18.05
$T_{total\_building}$ (min) in our system	3.5	17.97	21.75	46.27
$T_{total\_building}$ (min) in a commercial system	15	107	93.26	196

[a]$T_{projection}$ is the projection time of one layer except the layers for base.

waiting time is 0, a 0.1 s $T_{wait\_filling}$ is used to compensate any potential noises. A 0.05 mm/s velocity is used to lift the platform up. For models as shown in Figs. 7, 9, and 10, the layer thickness was set as 20 μm. A 0.55-s mask image projection time was used for each 20 μm layer except the base. The waiting time after mask image projection, $T_{wait\_projection}$, was set at 0.5 s. In addition, the solid cross section sizes of all the sliced layers are smaller than 6 mm even though their part dimensions may be bigger than 6 mm. Therefore, a 0.1 s $T_{wait\_filling}$ was used to fabricate all the following tests except the parallel plane model. Figure 8 shows a turbofan test case. In order to shape the curvature better, a smaller layer thickness, 12 μm, was used. Accordingly, a 0.4 s projection time, a 0.3 s projection waiting time $T_{wait\_projection}$, and a 2 s Z movement time are used for building each 12 μm layer. Figure 8(*b*) shows a microscopic image of the thin blades of the built part ($\sim$50 μm).

4.2 Build Speed Discussion. In the top–down projection-based MIP-μSL processes, it usually takes more than 20 s to recoat a thin layer of liquid resin for building next layers. However, with the discussed single-layer movement approach, the resin recoating time is less than 3.5 s for a 20 μm layer, which is much shorter than other MIP-μSL processes. Hence, a CAD model with microscale features can be fabricated in minutes instead of hours using the developed approach. Such a fabrication speed is much faster than the previously reported μSL work [19–23]. Table 1 shows the build time of our MIP-μSL system in fabricating some test parts, and how they compare with the building time of a commercial MIP-μSL system from EnvisionTEC (Dearborn, MI). Note that the same resin and resin curing time are used in both the commercial system and our system in the comparison.

5 Conclusion

A fast MIP-μSL process has been developed for the production of 3D microscale structures with complex geometries. The proposed micro-additive manufacturing technology is based on a bottom–up projection configuration using a single-layer movement approach. Process parameters have been optimized to avoid defects, while achieving the least resin recoating time. By using the one-layer gap distance and near zero waiting time, the resin recoating time can be reduced to 2–4 s in our system, making the total build time significantly shorter. The experimental results illustrate that the developed MIP-μSL process with single-layer movement can successfully fabricate 3D objects with complex geometry and microscale features in minutes.

Some future work that we are investigating includes: (1) developing a model for optimizing the resin recoating time, (2) refining the resolution of the MIP-μSL system; and (3) synchronizing the projection and resin recoating process to further speed up the building process.

References

[1] Varadan, V. K., Jiang, X., and Varadan, V. V., 2001, *Microstereolithography and Other Fabrication Techniques for 3D MEMS*, Wiley, DeKalb, IL, Chap. 1.
[2] Hirata, Y., 2003, "LIGA Process–Micromachining Technique Using Synchrotron Radiation Lithography–and Some Industrial Applications," Nucl. Instrum. Methods Phys. Res. Sect. B, **208**, pp. 21–26.
[3] Ikuta, K., and Hirowatari, K., 1993, "Real Three Dimensional Micro Fabrication Using Stereo Lithography and Metal Molding," An Investigation of Micro Structures, Sensors, Actuators, Machines and Systems, IEEE, Fort Lauderdale, FL, pp. 42–47.
[4] Ikuta, K., Ogata, T., Tsubio, M., and Kojima, S., 1996, "Development of Mass Productive Micro Stereo Lithography (Mass-IH Process)," An Investigation of Micro Structures, Sensors, Actuators, Machines and Systems, IEEE, San Diego, CA, pp. 301–306.
[5] Zhang, X., Jiang, X. N., and Sun, C., 1999, "Micro-Stereolithography of Polymeric and Ceramic Microstructures," Sens. Actuators A, **77**(2), pp. 149–156.
[6] Saxena, I., Malhotra, R., Ehmann, K., and Cao, J., 2015, "High-Speed Fabrication of Microchannels Using Line-Based Laser Induced Plasma Micromachining," J. Micro Nano Manuf., **3**(2), p. 021006.
[7] Saxena, I., Wolff, S., and Cao, J., 2015, "Unidirectional Magnetic Field Assisted Laser Induced Plasma Micro-Machining," Manuf. Lett., **3**, pp. 1–4.
[8] Cheng, Y. L., and Lee, M. L., 2009, "Development of Dynamic Masking Rapid Prototyping System for Application in Tissue Engineering," Rapid Prototyping J., **15**(1), pp. 29–41.
[9] Choi, J., Wicker, R., Lee, S., Choi, K., Ha, C., and Chung, I., 2009, "Fabrication of 3D Biocompatible/Biodegradable Micro-Scaffolds Using Dynamic Mask Projection Microstereolithography," J. Mater. Process. Technol., **209**(15), pp. 5494–5503.
[10] Ikuta, K., Hirowatari, K., and Ogata, T., 1994, "Three Dimensional Micro Integrated Fluid Systems (MIFS) Fabricated by Stereo Lithography," IEEE Workshop on Micro Electro Mechanical Systems, IEEE, Oiso, Japan, Jan. 25–28.
[11] Sun, C., Fang, N., Wu, D. M., and Zhang, X., 2005, "Projection Micro-Stereolithography Using Digital Micro-Mirror Dynamic Mask," Sens. Actuators A: Phys., **121**(1), pp. 113–120.
[12] Choi, J. S., Kang, H. W., Lee, I. H., Ko, T. J., and Cho, D. W., 2009, "Development of Micro-Stereolithography Technology Using a UV Lamp and Optical Fiber," Int. J. Adv. Manuf. Technol., **41**(3–4), pp. 281–286.
[13] Xu, G., Zhao, W., Tang, Y., and Lu, B., 2006, "Novel Stereolithography System for Small Size Objects," Rapid Prototyping J., **12**(1), pp. 12–17.
[14] Bártolo, P. J., ed., 2011, *Stereolithography: Materials, Processes and Applications*, Springer Science & Business Media, Berlin, Germany, Chap. 1.
[15] Hadipoespito, G. W., 2004, "Digital Micromirror Device (DMD) Based Integral Microstereolithography," Ph.D. thesis, University of Wisconsin-Madison, Madison, WI.
[16] Dendukuri, D., Pregibon, D. C., Collins, J., Hatton, T. A., and Doyle, P. S., 2006, "Continuous-Flow Lithography for High-Throughput Microparticle Synthesis," Nat. Mater., **5**(5), pp. 365–369.
[17] Pan, Y., Zhou, C., and Chen, Y., 2012, "A Fast Mask Projection Stereolithography Process for Fabricating Digital Models in Minutes," ASME J. Manuf. Sci. Eng., **134**(5), p. 051011.
[18] Limaye, A. S., and Rosen, D. W., 2007, "Process Planning Method for Mask Projection Micro-Stereolithography," Rapid Prototyping J., **13**(2), pp. 76–84.
[19] Choi, J. W., Ha, Y. M., Lee, S. H., and Choi, K. H., 2006, "Design of Microstereolithography System Based on Dynamic Image Projection for Fabrication of

Three-Dimensional Microstructures," J. Mech. Sci. Technol., **20**(12), pp. 2094–2104.
[20] Takagi, T., and Nakajima, N., 1994, "Architecture Combination by Micro Photoforming Process," IEEE Workshop on Micro Electro Mechanical Systems, IEEE, Oiso, Japan, pp. 211–216.
[21] Bertsch, A., Bernhard, P., Vogt, C., and Renaud, P., 2000, "Rapid Prototyping of Small Size Objects," Rapid Prototyping J., **6**(4), pp. 259–266.
[22] Monneret, S., Loubere, V., and Corbel, S., 1999, "Microstereolithography Using a Dynamic Mask Generator and a Noncoherent Visible Light Source," Design, Test, and Microfabrication of MEMS/MOEMS, International Society for Optics and Photonics, Paris, France, pp. 553–561.
[23] Monneret, S., Provin, C., and Le Gall, H., 2001, "Micro-Scale Rapid Prototyping by Stereolithography," 8th IEEE International Conference on Emerging Technologies and Factory Automation, Juan les Pins, France, Vol. 2, pp. 299–304.